

CMB constraints on U(1) Axion warm inflation

Asma Alaei^{a,*}, Sukannya Bhattacharya^{b,†} and Vahid Kamali^{acde‡}

^aDepartment of Physics, Bu-Ali Sina (Avicenna) University, Hamedan 65178, 016016, Iran

^bInstituto de Física Teórica UAM/CSIC, Calle Nicolás Cabrera 13-15, Cantoblanco, 28049, Madrid, Spain

^cDepartment of Physics, McGill University, Montréal, QC, H3A 2T8, Canada

^dSchool of Continuing Studies, McGill University, Montréal, QC, H3A 2T5, Canada

^eTrottier Space Institute, Department of Physics,
McGill University, Montréal, QC, H3A 2T8, Canada

In this work, we propose a model of warm inflation driven by axion-like particles interacting with $U(1)$ gauge fields, with implications for the early universe's thermal evolution. By extending traditional warm inflation models, we introduce a dissipation mechanism through the thermal fluctuations of electromagnetic fields, leading to a non-trivial backreaction on the inflaton's dynamics. Our results are consistent with CMB observations, even for a natural sub-Planckian Axion decay constant $f < M_p$. We present precise constraints on the model's free parameters, using CAMB and CosmoMC codes. These findings offer new insights into the thermal history of the universe and the nature of inflationary dynamics.

I. INTRODUCTION

While the standard inflation model provides an elegant framework for the early time evolution of the universe [1–4], certain aspects of the model building, as well as the details of the reheating mechanism following inflation remain poorly understood despite continued theoretical efforts [5–12].

As a modification of the standard cold inflation paradigm, the motivation for warm inflation is to realise inflation in a more general setting where the *inflaton* field co-exists with radiation, while the energy stored in the inflaton field continuously dissipates into radiation [13–15]. This dissipation can occur through interactions with other fields, leading to a thermal bath that modifies the background and perturbations of inflation dynamics. Warm inflation is thus a natural extension of the standard inflationary paradigm, where the inflaton field not only drives accelerated expansion but also efficiently transfers energy to radiation, maintaining a non-zero temperature throughout the inflationary phase, hence allowing for a smooth transition from inflation to reheating. The modifications to the power spectrum of primordial perturbations in the warm setup can also be constrained with the CMB data [16–35].

The interaction of the inflaton with the fields in the thermal bath to realise such dissipation is, however, a crucial part of the model building to preserve the flatness of the potential. Light mediators, e.g. fermions, can introduce large thermal corrections to the inflaton potential, ruining slow-roll; however such models can be realised with additional symmetries (ref. Little Higgs). Heavy mediators preserve the flatness of the inflaton potential, however, can only lead to sizeable dissipation when present in large quantities. Recently, warm inflation models have gained significant attention in the context of axion-like particles, which arise in several high-energy theories, including string theory and various

models of particle physics beyond the Standard Model [20, 21, 32, 34, 36–41]. Axions, which are pseudoscalar particles, interacting with (non-)Abelian gauge fields, could provide a thermal radiation bath during inflation. It has been explored in previous studies [42, 43].

In this paper, we propose a model of warm inflation in which the interaction between axion inflaton and $U(1)$ gauge fields generates a thermal bath during inflation [44], and a sub-Planckian decay constant is able to achieve enough number of e-folds and observationally compatible model [45].¹ In particular, here, the plasma consists of $U(1)$ gauge fields, which is continuously replenished by axion decay and we investigate the *thermal backreaction* of the plasma on the evolution of the inflaton. Our setup also includes fermions charged under the $U(1)$ gauge field, which are crucial for achieving a thermalized plasma and analyzing its backreaction on the inflaton dynamics. [49, 50].

By representing the Chern-Simons term with a thermal average of the local fluctuations of the electromagnetic fields, we utilize the linear response method and real-time thermal field theory [51–53] to quantify the dissipation. This approach allows us to model the thermal influence on the background of the system and evaluate a power spectrum for the dominant thermal fluctuations. This is an interesting approach, since the gauge field fluctuations reach large amplitudes within an instability band closer to horizon exit [54–64], and limits on backreaction of the gauge fields on the axion are typically studied in

¹ Similar scenarios of warm inflation has been realised in previous literature with cosine potential where inflaton is a pNGB coupled to another pNGB field [46] and in the context of $SU(N)$ gauge fields coupled to axions [21, 34, 36, 47]. See [14] for a concrete model of *warm little inflation* by directly coupling the inflaton (pNGB) to a few light fermions. References [48] and [41] derived limits for thermalization in axion inflation coupled to $U(1)$ and $SU(2)$ gauge fields respectively.

the context of cold inflation paradigm [65–73]. Our approach assumes thermalization, in fact thermalised initial conditions, and the thermal bath prevails exponential expansion.

To check the consistency with data, we constrain our model with the latest CMB data (Planck 2018) using MCMC simulations² to find the best fit values of the model parameters. These tools allow us to derive precise constraints on key parameters, such as the axion decay constant f , the axion mass m_ϕ , and the dissipation parameter Q . Interestingly, Q arises from the thermal backreactions, and therefore it is directly linked to the Chern-Simons term. It is worth noting here that we assume the backreaction to be large enough so that thermalization is possible, but not strong enough to ruin slow-roll, at least at CMB scales. Our results provide new insights into the possibility of thermal effects present during inflation and the potential signatures of warm inflationary models in the CMB.

In Section II, we present our setup and considering thermal treatment of the backreaction, reach an expression for the dissipation coefficient. In Section III, the system is presented in the warm paradigm with the background evolution and warm power spectrum. In Section IV, we confront our setup with the latest CMB data and constrain the model parameters. In Section V we conclude our analysis and discuss our results for the parameters in view of existing bounds in the literature.

II. THE MODEL

The Lagrangian of the model contains axion ϕ as the inflaton and fermions ψ charged under U(1) gauge-fields A_μ and a Chern-Simons coupling between inflaton and gauged fields in a curved space-time:

$$\mathcal{L} = \sqrt{-g} \left[-\frac{R}{2} - \frac{1}{2} F_{\mu\nu} F^{\mu\nu} - \frac{1}{2} (\partial_\mu \phi)^2 - V(\phi) \right] \quad (1)$$

$$+ \bar{\psi} (i\cancel{D} - m_f) \psi - \frac{\lambda}{4\pi f} \phi F_{\mu\nu} \tilde{F}^{\mu\nu}$$

where $F_{\mu\nu} \equiv \partial_\mu A_\nu - \partial_\nu A_\mu$ is the U(1) field strength, while $\tilde{F}^{\mu\nu} \equiv \frac{1}{2} \frac{\epsilon^{\mu\nu\alpha\beta}}{\sqrt{-g}} F_{\alpha\beta}$ is its dual, with $\epsilon^{\mu\nu\alpha\beta}$ totally anti-symmetric (and $\epsilon^{0123} = +1$). g the determinant of the underlying FLRW metric with the line element $ds^2 = -dt^2 + a^2(t)d\vec{x}^2$, $a(t)$ being the scale factor. We consider the following periodic potential for the scalar field

$$V(\phi) = m_\phi^2 f^2 \left(1 + \cos \left(\frac{\phi}{f} \right) \right), \quad (2)$$

² We use CAMB (Code for Anisotropies in the Microwave Background) and CosmoMC (Cosmological Monte Carlo) codes, which are widely used to calculate the CMB power spectrum and constrain cosmological parameters.

where the shift symmetry protects it from thermal corrections. m_ϕ is axion mass and f is decay constant. We will study our model in natural units, $\hbar = c = \kappa_b = 1$.

Variation of the above Lagrangian (1) with respect to the scalar field leads to the following modified Klein-Gordon equation for the axion background

$$\ddot{\phi} + 3H\dot{\phi} + V_\phi(\phi) = \frac{\lambda}{2\pi f} \langle \vec{E} \cdot \vec{B} \rangle, \quad (3)$$

where $V_\phi(\phi) = \frac{dV}{d\phi}$ and the source term on the right-hand side of Eq.(3) can produce a thermal bath through dissipation. This system has two important pictures of the thermal process according to their physical origin. The first one includes the scattering between axion and gauge fields that normally leads to a weak dissipative regime of warm inflation where the backreaction term, i.e the R.H.S of Eq.(3), is negligible at the background level [74]. The second one, which we are interested in this work, involves a collective dissipative effect of the thermal bath of gauge fields.

To study the thermal backreaction of the plasma on the evolution of the axion, we replace the Chern-Simons term $\vec{E} \cdot \vec{B}$ in Eq.(3) by the thermal average of the local fluctuations of the electromagnetic fields, $\langle \vec{E} \cdot \vec{B} \rangle$, and utilize the linear response method in the context of real-time thermal field theory [51] (see Appendix A).

$$\frac{\lambda}{2\pi f} \langle \vec{E} \cdot \vec{B} \rangle = \frac{\lambda}{2\pi f} \langle \vec{E} \cdot \vec{B} \rangle_0 + \int d^4x' \Sigma_R(x-x') \delta\phi(t'). \quad (4)$$

Here, $\Sigma_R(x-x')$ is a retarded correlation of the fields, containing non-local information, which depends on the interaction Lagrangian \mathcal{L}_{int} , related to the retarded Green's function $\Sigma_\rho(x-x')$ as:

$$\Sigma_R(x-x') = \Theta(t-t') \Sigma_\rho(x-x') \quad (5)$$

$$\Sigma_\rho(x-x') = i \left(\frac{\partial f(\phi)}{\partial \phi} \right)^2 \langle [g(X(x)), g(X(x'))] \rangle, \quad (6)$$

where,

$$\mathcal{L}_{\text{int}} = f(\phi)g(X),$$

X being the radiation component.

In case of the Lagrangian in Eq. 1, therefore,

$$\Sigma_\rho(x-x') = -i \frac{\lambda^2}{4\pi^2 f^2} \langle [(\vec{E} \cdot \vec{B})(x), (\vec{E} \cdot \vec{B})(x')] \rangle. \quad (7)$$

At the level of no interaction specified by zero index, the CP conservation vanishes the first term in eq.(4), so that,

$$\frac{\lambda}{2\pi f} \langle \vec{E} \cdot \vec{B} \rangle = -i \frac{\lambda^2}{4\pi^2 f^2} \int dt' \Theta(t-t') \quad (8)$$

$$\times \int d^3x' \langle [(\vec{E} \cdot \vec{B})(x), (\vec{E} \cdot \vec{B})(x')] \rangle.$$

In the adiabatic approximation, when the inflaton is varying on a much larger timescale than the response (or

relaxation) time of dissipation, i.e., $\frac{\dot{\phi}}{\phi} \ll \tau^{-1}$, then the source term of Eq. 3, i.e. $\frac{\lambda}{2\pi f} \langle \vec{E} \cdot \vec{B} \rangle$ can be written in the form of a friction term $\Upsilon \dot{\phi}$ in the background equation:

$$\ddot{\phi} + (3H + \Upsilon)\dot{\phi} + V_\phi(\phi) = 0. \quad (9)$$

The dissipation parameter Υ is in general a function of ϕ and temperature T , and is responsible for transferring the kinetic energy of inflaton (axion) to the radiation (gauge field) sector. It is possible to find the form of Υ from the retarded green function $\Sigma_\rho(x - x')$ [75].

$$\Upsilon = i \lim_{\omega \rightarrow 0} \frac{\partial \tilde{\Sigma}_\rho(\omega, 0)}{\partial \omega}, \quad (10)$$

$$\text{where,} \quad (11)$$

$$\tilde{\Sigma}_\rho(\omega, \vec{k}) = \int d^4y \Sigma_\rho(t, \vec{y}) e^{-i\omega t} e^{i\vec{k} \cdot \vec{y}}.$$

The retarded Green function $\Sigma_\rho(x - x')$ contains all the information related to back-reaction in the thermal setting, which can be evaluated for our case in terms of $\beta = 1/T$ as (see Appendix A)

$$\begin{aligned} \tilde{\Sigma}_\rho(\omega, \vec{k}) &= -i \frac{\lambda^2}{4\pi^2 f^2} (1 - e^{-\beta\omega}) \\ &\times \epsilon^{\alpha\beta\gamma\tau} \epsilon^{\mu\nu\rho\sigma} \langle \partial_\alpha A_\beta \partial_\gamma A_\tau \partial'_\mu A_\nu \partial'_\rho A_\sigma \rangle \\ &= -i \frac{\lambda^2 \omega}{768\pi^3 f^2} \left(\omega^2 - m_D^2 \right)^{1/2} \left(\omega^2 + 2m_D^2 \right) \\ &\times (1 - e^{-\beta\omega}) \left[\frac{1}{e^{\beta\omega/2} - 1} + \frac{1}{(e^{\beta\omega/2} - 1)^2} \right] \end{aligned} \quad (12)$$

Here, m_D is the thermal mass, that can be written in terms of the Debye length [49] $m_D \sim \lambda_D^{-1} \sim eT$, where e is the fermionic charge. The fermionic mass doesn't appear in this expression since the plasma temperature is substantially greater than the fermionic mass so that the thermal bath is relativistic. To find the above form of the correlation function, we have used the tree-level calculation in thermal field theory [51]. Using the expression in (10),

$$\Upsilon = \frac{e^3}{192\pi^3} \frac{\lambda^2}{f^2} T^3 \quad (13)$$

Therefore, the dissipation parameter obtained here is cubic in temperature. Correspondingly,

$$Q \equiv \frac{\Upsilon}{3H} = \frac{e^3}{576\pi^3} \frac{\lambda^2}{f^2} \frac{T^3}{H} \quad (14)$$

We will show in the next section that in the adiabatic limit, we can consider Q to be nearly constant.

III. WARM INFLATION

The evolution of the background axion field is now given in Eq. 9, which, together with the evolution of the

radiation energy density ρ_R and the Friedman equation, completely contain the background information.

$$\dot{\rho}_R + 4H\rho_R = 3HQ\dot{\phi}^2 \quad (15)$$

$$H^2 = \frac{1}{3M_{\text{Pl}}^2} (V(\phi) + \frac{\dot{\phi}^2}{2} + \rho_R) \quad (16)$$

These are the most general equations for warm inflation driven by a single field potential $V(\phi)$ for the inflaton ϕ . Under the assumption of slow-rolling ϕ (assumed in adiabatic condition to calculate Υ), slowly varying ρ_R , and noting that $\rho_R, \frac{\dot{\phi}^2}{2} \ll V(\phi)$ during inflation, the above Eq.s lead to

$$\dot{\phi}^2 = \frac{V_\phi^2}{3H^2} \frac{1}{3(1+Q)^2} = \frac{2V\epsilon_V}{3(1+Q)^2}, \quad (17)$$

$$\rho_R = \frac{3Q}{4} \dot{\phi}^2 = M_{\text{Pl}}^2 \frac{V_\phi^2}{4V} \frac{Q}{(1+Q)^2} = \frac{V\epsilon_V}{2} \frac{Q}{(1+Q)^2} \quad (18)$$

where $\epsilon_V \equiv \frac{M_{\text{Pl}}^2}{2} \left(\frac{V_\phi}{V} \right)^2$ is the usual slow-roll parameter.

Using $\rho_R = C_R T^4$, where $C_R = \frac{\pi^2}{30} g_*(T)$, the temperature can be calculated as

$$T = \left(\frac{V\epsilon_V}{2C_R} \right)^{1/4} \frac{Q^{1/4}}{(1+Q)^{1/2}}. \quad (19)$$

Combining this expression of T with $H^2 = V/3M_{\text{Pl}}^2$ in the slow roll limit,

$$Q = C_Q \lambda^{8/7} \left(\frac{m_\phi}{f} \right)^{2/7} \left(\frac{f}{M_{\text{Pl}}} \right)^{-10/7} \left[\frac{\sin^3(\phi/2f)}{\cos^2(\phi/2f)} \right]^{2/7} \quad (20)$$

$$\text{where } C_Q = \left(\frac{e^3}{576\pi^3} \right)^{4/7} \frac{3^{2/7}}{C_R^{3/7} 2^{5/7}}.$$

Due to the weak dependence on the factor in the square bracket, Q remains nearly constant during inflation. For this reason, in the rest of our analysis, we have considered Q to be a constant.

In this warm setup with a sustaining radiation bath with subdominant energy density, inflation ends with the end of effective slow-roll, i.e., when $\frac{\epsilon}{1+Q} = 1$ where $\epsilon = -\frac{\dot{H}}{H^2} \simeq \epsilon_V$. The evolution of energy densities for a benchmark point with constant $Q = 200$, $f = 0.5M_{\text{Pl}}$, $m_\phi = 2.5 \times 10^{-8}M_{\text{Pl}}$ and for 55 inflationary e-folds has been shown in Fig. 1, which shows that inflation indeed ends with the kinetic energy overtaking the potential energy, while the radiation energy density still remains subdominant at the end of inflation. Furthermore, we work in the large dissipation regime, $Q \gg 1$ which is consistent with an ultra-relativistic thermal plasma, and ensures $\rho_R \ll V(\phi)/2$ from Eq. (17).

The number of e-folds from when a mode k exits the inflationary horizon at e-fold $N(k)$ until the end of inflation at N_e at the field value ϕ_e for the periodic potential

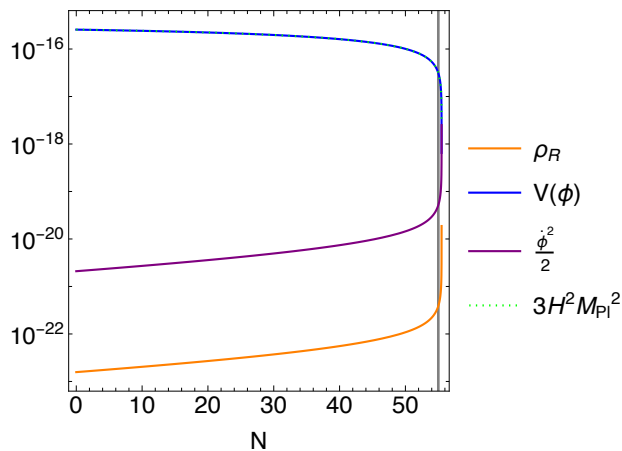


FIG. 1: Evolution of potential, kinetic and radiation energy densities (all in units of $|Mp^4$) plotted in blue, purple and orange solid lines for the benchmark point $Q = 200$, $f = 0.5M_{Pl}$, $m_\phi = 2.5 \times 10^{-8}M_{Pl}$ and for 55 inflationary e-folds. The Hubble parameter is shown with dotted green line and the end of inflation is shown with the vertical gray line.

(2) is then

$$N_e - N(k) = \int_N^{N_e} dN = \gamma^2 \ln \left[\sin\left(\frac{\phi}{2f}\right) \Big|_{\phi_e}^{\phi_e} \right], \quad (21)$$

where

$$\gamma^2 \equiv \frac{2f^2 Q}{M_{Pl}^2}. \quad (22)$$

Using the condition $\epsilon(\phi_e)/Q = 1$ at the end of inflation, $\sin^2(\phi_e/2f) = \frac{\gamma^2}{1+\gamma^2}$, so that³ using Eq. 21,

$$\sin(\phi/2f) = \frac{\gamma}{\sqrt{1+\gamma^2}} \exp\left(\frac{N-N_e}{\gamma^2}\right). \quad (23)$$

The scalar power spectrum in warm inflation has contributions from both vacuum and thermal fluctuations⁴.

$$\mathcal{P}_R \simeq \left(\frac{H}{\dot{\phi}}\right)^2 \frac{H^2}{(2\pi)^2} \left[1 + \frac{T}{H} \frac{2\pi Q}{\sqrt{1+4\pi Q/3}}\right]. \quad (24)$$

The power spectrum can be estimated for the case of strong dissipative regime $Q \gg 1$, where the thermal fluc-

tuations dominate.

$$\mathcal{P}_R = \frac{Q^{\frac{9}{4}} V^{\frac{9}{4}}}{4\sqrt{2\pi^3} C_R^{\frac{1}{4}} M_{Pl}^{\frac{9}{2}} V_{,\phi}^{\frac{3}{2}}} \quad (25)$$

$$= P_0 \frac{m_\phi}{f} \frac{\gamma^{\frac{9}{2}}}{g(\gamma)^{\frac{3}{4}}} \left[\chi(N, \gamma) - \frac{g(\gamma)}{\chi(N, \gamma)} \right]^{\frac{3}{2}}, \quad (26)$$

$$\text{where } P_0 = \frac{1}{16\pi^{\frac{3}{2}} C_R^{\frac{1}{4}}}$$

$$g(\gamma) = \frac{\gamma^2}{1+\gamma^2}, \quad \text{and } \chi(N, \gamma) = \exp\left[\frac{N_e - N}{\gamma^2}\right].$$

The second expression for the power spectrum in Eq. (26) is expressed completely in terms of model parameters m_ϕ, f, γ , and number of e-folds using Eq. 23.

The CMB pivot scale $k_p = 0.05 \text{ Mpc}^{-1}$, crosses the horizon at N_p so that $k_p = a(N_p)H(N_p)$, and therefore, $N_e - N(k) = N_{\text{inf}} - \log(k/k_p)$, where $N_{\text{inf}} \equiv N_e - N_p$ is the total number of e-folds of inflation between the horizon exit of the pivot scale and end of inflation. The scalar power spectrum in Eq. 26 can thus be written incorporating the scale dependence as

$$\mathcal{P}(k) = P_0 \left(\frac{m_\phi}{f}\right)^{\frac{3}{2}} \frac{\gamma^{\frac{9}{2}}}{g(\gamma)^{\frac{3}{4}}} \left[\bar{\chi}(k, \gamma) - \frac{g(\gamma)}{\bar{\chi}(k, \gamma)} \right]^{\frac{3}{2}} \quad (27)$$

where

$$\bar{\chi}(k, \gamma) = \left(\frac{k}{k_p}\right)^{-\frac{1}{\gamma^2}} \exp[N_{\text{inf}}/\gamma^2].$$

Using this form of the power spectrum, the amplitude and spectral index at the pivot scale are

$$A_w = P_0 \left(\frac{m_\phi}{f}\right)^{\frac{3}{2}} \frac{\gamma^{\frac{9}{2}}}{g(\gamma)^{\frac{3}{4}}} \left[\bar{\chi}(k_p, \gamma) - \frac{g(\gamma)}{\bar{\chi}(k_p, \gamma)} \right]^{\frac{3}{2}} \quad (28)$$

and

$$n_w - 1 \equiv \left. \frac{d \log \mathcal{P}(k)}{d \log k} \right|_{k=k_p} = -\frac{3}{2\gamma^2} \frac{\bar{\chi}^2(k_p, \gamma) + g(\gamma)}{\bar{\chi}^2(k_p, \gamma) - g(\gamma)} \quad (29)$$

It is interesting to note that the scalar spectral index depends only on the parameter γ for a given number of inflationary e-folds. In Fig. 2, n_w is plotted with γ for two values of inflationary number of e-folds. Fig. 2 shows that CMB constraints are expected to be satisfied for $\gamma^2 \sim \mathcal{O}(100)$, which can be obtained for sub-Planckian f only in the strong dissipative regime.

With these equations and estimates, we are now ready to enter our model in CAMB with a viable prior range and test it using CMB data.

IV. ANALYSIS

We analyse our model by implementing the power spectrum in Eq.27 in the cosmological Boltzmann code CAMB [78, 79]. We fix the value of N_{inf} and find the

³ Note that, we calculate the number of e-folds forward in time, i.e., $N_e > N(k)$, and therefore $\sin(\phi/2f) < \sin(\phi_e/2f)$, which can be understood remembering that we evolve ϕ/f in the first quadrant, and ϕ increases as inflation progresses.

⁴ We do not consider here the effect on the power spectrum (represented by $G(Q_*)$ in [14]) due to the coupling of the scalar fluctuations to radiation fluctuations, which we assume to have negligible effect near the CMB scales.

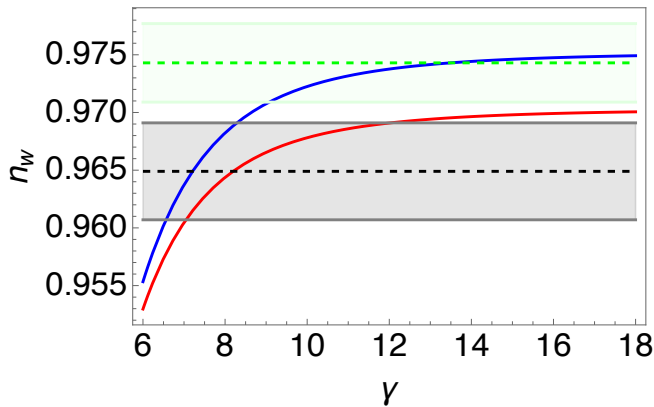


FIG. 2: Evolution of n_w for $N_{\text{inf}} = 50$ and 60 plotted with red and blue lines respectively. The marginalised values of the spectral index from Planck 2018 [76] $n_s = 0.9649 \pm 0.0042$ and from P-ACT-LB [77] (CMB lensing from ACT and Planck and BAO data from DESI Y1) $n_s = 0.9743 \pm 0.0034$ are shown with black and green dashed lines respectively. The corresponding 1σ limits are shown with gray and green shaded regions respectively.

best fit values of the parameters γ and m_ϕ/f . For our cosmological analysis, we constrain the inflation parameters alongside the late time cosmological parameters $\{\Omega_b h^2, \Omega_c h^2, \theta, \tau\}$ using the following datasets:

- *Planck* 2018 TT + TE +EE with low ℓ and low E likelihood [18];
- *Planck* 2018 lensing likelihood [80];
- SDSS BAO likelihood [81].

The likelihoods are sampled using the MCMC sampler [82, 83], through its interface with `CosmoMC`. We sample the likelihoods until we reach a value $R - 1 = 0.05$ for the Gelman-Rubin diagnostic. The resulting chains are analysed and plotted with `GetDist` [84]. At the end of the sampling, we also run a minimizer to find the best-fit point and the corresponding χ^2 values.

From Eq. 27, it is evident that the power spectrum depends only on the following combinations of the model parameters: $\frac{m_\phi}{f}$ and $f^2 Q$. For this reason, and noting that the amplitude of scalar power spectrum has stringent constraints from CMB, we choose to vary the following combinations of the model parameters in CAMB: $\ln(10^{10} m_\phi/f)$ and $\gamma/100$.

In Fig. 3 we plot the two-dimensional posterior probability distribution for the derived parameters $\frac{m_\phi}{f}$ and $f^2 Q$ for $N_{\text{inf}} = 50$ and 60 , and quote their best-fit values and 1σ confidence limits in Table I. Figure (7) and Table II in the Appendix B present the posterior probability distribution of all 6 cosmological parameters and

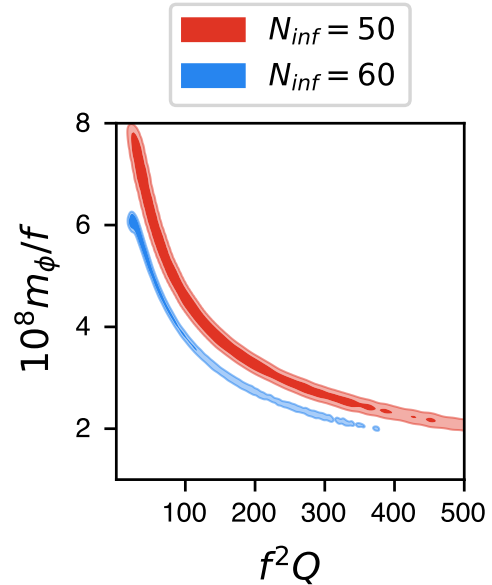


FIG. 3: 2D posterior distribution of the derived model parameters.

TABLE I: Best-fit values of key model parameters derived from the analysis

N_{inf}	50	60
$f^2 Q/M_{\text{Pl}}^2$	101	32
m_ϕ/f	4.57×10^{-8}	5.85×10^{-8}

their mean values with 1σ confidence limits (along with best-fit values) respectively.

Evidently, m_ϕ/f is well-constrained for both the cases $N_{\text{inf}} = 50$ and 60 , whereas γ and therefore $f^2 Q$ remains poorly constrained. Indeed, as mentioned earlier, the amplitude and the spectral index of the scalar power spectrum (Eq.s (28) and (29)) depend on the model parameters such that n_w depends only on γ , and the order of A_w is mainly determined by m_ϕ/f with only weak dependence on γ . Furthermore, n_w asymptotes to a N_{inf} -dependent value for large γ , given by

$$n_w|_{\gamma \gg 1} \simeq \frac{2(N_{\text{inf}} - 1)}{2N_{\text{inf}} + 1}. \quad (30)$$

This is the reason for the posterior 1D distribution of γ (Fig. 7) or the 2D posterior distribution of the derived quantity $f^2 Q$ (Fig. 3) to have a sharp cutoff at small values, and wide tails for large values.

V. CONCLUSIONS AND DISCUSSIONS

In this work, we explored the constraints from CMB observations on the axion $U(1)$ inflation realized in the

warm paradigm. Starting from the equation of motion (3), we have assumed the source due to the large fluctuations in the gauge sector to be thermal. Thus, the source term leads to the dissipation from the inflaton field to the electromagnetic sector, containing gauge fields and fermions, with a dissipation coefficient Υ , which is estimated in Eq. (13) using linear response method. The result for the dissipation coefficient in warm axion $U(1)$ inflation is the novelty of our work.

The form of the dissipation coefficient Υ is illuminating further than the cubic dependence on temperature found in our scenario. The fermion mass doesn't appear explicitly in this expression (13) since the plasma is ultra-relativistic. However, the contribution of the fermion is important, since it induces thermal mass to the gauge field, which contributes to the dissipation as $\Upsilon \propto m_D^3$. This dependence on the thermal mass clearly indicates that a simpler scenario, with no fermions present (e.g. for a dark $U(1)$ sector), and therefore $m_D = 0$, the dissipation coefficient is vanishing. In other words, fermions play a crucial role in our setup by inducing a thermal mass of the photons which directly leads to a non-zero thermal dissipation.

Furthermore, the Chern-Simon's coupling is dependent on the fermionic charge e , such that $\lambda = \mathbf{q}\alpha$ with $\alpha \equiv e^2/4\pi$, where \mathbf{q} is a constant that varies from model to model [85]. Therefore, $\Upsilon \propto e^7$ from Eq. (13), hinting at the possibility for strong dissipation for large e , which is shown explicitly when discussing Fig. 4. This behaviour of $\Upsilon(e)$ can be compared to $\Upsilon \propto g^{10}$ found for the case of thermal sphaleron transitions for the case of non-Abelian gauge fields [37, 52, 86].

With the justified assumption of a constant temperature, hence constant Q , as discussed with Eq. (20), we proceed to find the dependence of the inflationary power spectrum on the model parameters (Eq. (27)). Using this expression in the CAMB code, we then constrain the parameters with CosmoMC, using cosmological data as listed in section IV. Our result shows the preferred posterior distribution for the combination of parameters m_ϕ/f and f^2Q . We found that m_ϕ/f is well constrained, however, for f^2Q there is a sharp cutoff at lower values, whereas larger values are possible with small probability.

Given our results for best-fit values for f^2Q , and from the dependence of Q on f , we can specifically check the region in the parameter space where large dissipation $Q \gg 1$ is possible. For constant Q , the part in the square bracket in Eq. (20) can be written completely in terms of γ and N_{inf} using Eq. (23). Now, to check the parametric dependence of Q , it is important to fix the charge e of the fermion, which is not necessarily a SM fermion, but can belong to a dark $U(1)$ sector. To account for an unknown e , in Fig. 4 we show the contour plots for Q with different values of $\lambda e^{3/2}$ and sub-Planckian f . for $N_{\text{inf}} = 60$, using

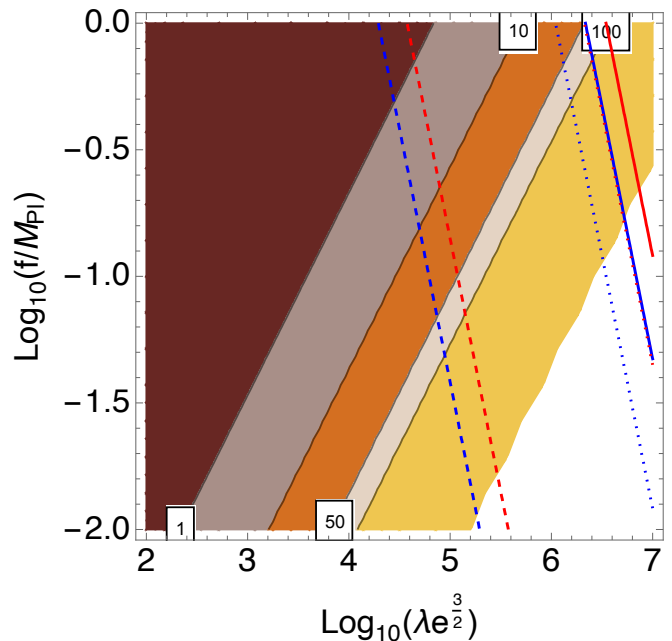


FIG. 4: Contour plot for Q for $Q = 1, 10, 50, 100$ are shown with $\lambda e^{3/2}$ and f . Red ($N_{\text{inf}} = 50$) and blue ($N_{\text{inf}} = 60$) lines are plotted for the mean values (solid lines), best-fit values (dotted lines) and (mean-2 σ) values (dashed lines) of γ and m_ϕ/f .

Eq. (14)⁵. The contours are plotted for the benchmark point⁶ $\gamma = 10$ and $m_\phi/f = 5 \times 10^{-8}$ with $N_{\text{inf}} = 55$. These *theory contours* shown at $Q = 1, 10, 50, 100$ come solely from parametric dependence of Q , and does not use any information from the constraints obtained from MCMC analysis. In the same figure, we have also plotted the contours for Q obtained using $Q = \frac{\gamma^2 M_{\text{Pl}}^2}{2f^2}$ in Eq. (20) and using the values of γ and m_ϕ/f obtained from MCMC analysis (see table II). These *constraint contours* are plotted in red ($N_{\text{inf}} = 50$) and blue ($N_{\text{inf}} = 60$) for the mean values (solid lines), best-fit values (dotted lines) of γ and m_ϕ/f . The dashed red and blue lines are plotted for the values of γ that are 2 σ smaller than the mean values⁷.

This figure gives us a clear idea of the parameter space viable for λ that can lead to strong dissipation with sub-Planckian f . The intersections of the *theory* and *constraint* contours in this figure show that it is possible to achieve $Q \gg 1$ for sub-Planckian f , but only for moderate to large values of $\lambda e^{3/2}$. Furthermore, the lower f is

⁵ We use $C_R = 65.5$ throughout this work, since it corresponds to $g_* = 200$.

⁶ This benchmark point is the same for which Fig. 1 is plotted before.

⁷ See Fig. 6 in Appendix B for a similar figure where the theoretical contours are also plotted using results from MCMC analysis with the mean values of γ and m_ϕ/f for different N_{inf} .

aimed, the larger is the required λ to satisfy CMB constraints. The range of γ between its mean value (solid red and blue lines) and lower 2σ ends (dashed red and blue lines) cover a range of $10^4 \lesssim \lambda e^{3/2} \lesssim 10^6$. Interestingly, this is the lower end of the posterior distribution of γ , which has a sharp cut-off as opposed to the long tail at large γ , and therefore the dashed red and blue lines indeed represent the lowest possible $\lambda e^{3/2}$ allowed by CMB data for a given N_{inf} . Moreover, using $e \gtrsim \mathcal{O}(1)$ can lead to $\lambda \sim \mathcal{O}(10 - 1000)$.

It is important to point out here that while deriving the dissipation coefficient using linear response theory, we have not used the linear solution for the gauge modes A_μ . The only assumption that is necessary for that derivation is the presence of large and homogeneous back-reaction, so that the inflaton still follows slow-roll dynamics. Nevertheless, it is interesting to investigate the status of the ‘particle production’ parameter $\xi \equiv \frac{\lambda \dot{\phi}}{2fH}$, that signifies the instabilities of the gauge fields. Rewriting the first slow roll equation (17) in the limit of large Q as

$$\frac{\dot{\phi}}{H} \simeq \frac{M_{\text{Pl}}^2}{fQ} \tan(\phi/2f), \quad (31)$$

leads to the following parametric dependence of ξ

$$\xi = \frac{\lambda}{\gamma^2} \tan(\phi/2f). \quad (32)$$

Given a particular pivot e-fold N_{inf} , and coupling constant λ , the value of ξ can be therefore estimated at a particular time signifying e-fold N during inflation, using Eq. (32) and (23). Using the mean values of γ obtained from MCMC analysis, ξ turns out to be explicitly dependent only on λ and N_{inf} , since $\tan(\phi/2f)$ depends directly on γ with the assumption of a constant Q .

In Fig. 5 ξ and $f/\lambda H$ are shown for the range $30 \lesssim \lambda \lesssim 10^4$ for two different sub-Planckian values of f . In cold axion inflation, there are limits on ξ e.g. from non-Gaussianity ($\xi \lesssim 2.5$), back-reaction ($\xi \lesssim 4.7$) and perturbativity ($\xi \lesssim 4.4$). The bounds are also plotted as vertical black, green and orange lines for back-reaction, non-Gaussianity and perturbativity respectively in Fig. 5.

Ref. [48] has discussed the bounds on ξ in the ξ - $f/\lambda H$ space for the onset of a thermal (warm) paradigm during axion- $U(1)$ inflation, including the backreaction and perturbativity bounds discussed above, charting the parameter space where it is possible to thermalize (with and without fermionic interactions)⁸. The limit $\xi \gtrsim 2.9$ found in their analysis to satisfy SM thermalization is also included in Fig. 5 as the magenta vertical line. Comparing our Fig. 5 in the context of those bounds, we find that

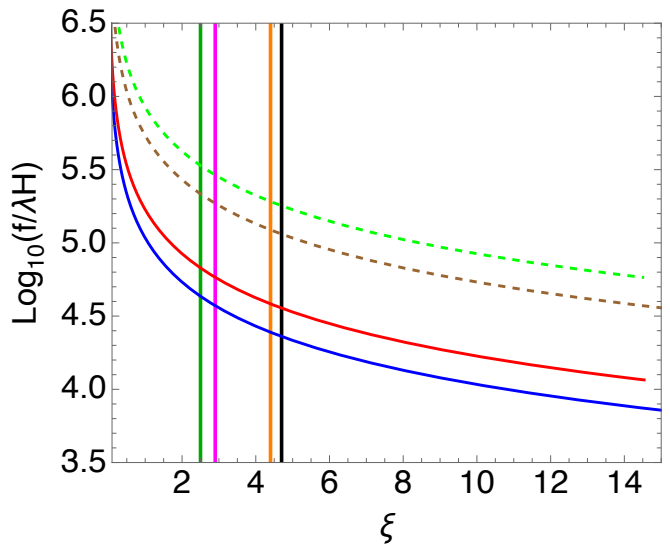


FIG. 5: Parametric dependence in the ξ - $f/\lambda H$ space on λ for $f = 0.5M_{\text{Pl}}$ (solid red and blue) and $f = 0.1M_{\text{Pl}}$ (dashed brown and green) respectively are plotted for $N_{\text{inf}} = 50$ (red and brown) and 60 (blue and green) lines respectively. Vertical black, green, orange, and magenta lines for back-reaction, non-Gaussianity, perturbativity, and thermalization respectively.

depending on the exact value of λ and e , the possible ξ and $f/\lambda H$ values in our case can belong to a regime where it is possible to thermalize via fermionic interactions and Chern-Simons coupling within the bounds of backreaction and perturbativity for a small range of λ , depending on the exact value of f/M_{Pl} .

However, these bounds are calculated using the gauge field solutions assuming small backreaction, and using the quantum vacuum fluctuations to determine the primordial power spectrum at CMB scales, whereas the primordial power spectrum is a thermal one in our case. Hence it is arguable whether these bounds directly apply to our analysis or not. Furthermore, the bounds in ref. [48] are derived assuming a cold (non-thermal) initial condition to reach conditions on the parameter space for attaining thermalization during inflation, whereas in this work we have assumed thermalization as an initial condition itself. Nevertheless, it is interesting to explore the relevant parameter space for our case to comment on the validity of the assumption of thermalization. The observations made about Fig. 5 above justify our assumption in the context of the relevant parameter space that have been explored for thermalization during axion $U(1)$ inflation in [48].

The requirement for fairly large λ and large $e \sim \mathcal{O}(1)$ is expected, since the concept of thermalization goes hand in hand with large couplings. On the other hand, ξ can still safely abide by the constraints on strong backreaction and perturbativity. This is an important result, val-

⁸ In [48] $\lambda = 1$, and therefore in our context the y-axis of their Figure 4 should be $f/\lambda H$ instead of f/H .

idating our a priori assumption for the thermalization of the $U(1)$ gauge fields in this axion inflation setup, with comments on the limitations on the parameters f and λ .

For non-Abelian gauge fields, recently [47] have explored a the chromonatural inflation model assuming a priori thermalization, whereas [41] have explored the limits in the parameter space where such an assumption is justified. For both Abelian and non-Abelian gauge fields present during axion inflation, the exact evolution from a cold to warm scenario either before or after the horizon exit of the pivot scale during inflation is however an important piece of the puzzle that is yet to be explored.

ACKNOWLEDGEMENT

SB acknowledges the ‘‘Consolidaci3n Investigadora’’ grant CNS2022-135590 and the support from the Spanish Research Agency (Agencia Estatal de Investigaci3n) through the Grant IFT Centro de Excelencia Severo Ochoa No CEX2020-001007-S, funded by MCIN/AEI/10.13039/501100011033. AA, SB and VK thank R. Brandenberger, M. Fasiello, and A. Papageorgiou for illuminating discussions and helpful comments.

* aasmaalaei6999@gmail.com

† sukannya.bhattacharya@ift.csic.es

‡ vahid.kamali2@mcgill.ca

- [1] A. A. Starobinsky, *Adv. Ser. Astrophys. Cosmol.* **3**, 130 (1987).
- [2] A. H. Guth, *Phys. Rev.* **D23**, 347 (1981).
- [3] A. Albrecht and P. J. Steinhardt, *Phys. Rev. Lett.* **48**, 1220 (1982).
- [4] A. D. Linde, *Phys. Lett. B* **108**, 389 (1982).
- [5] L. Kofman, A. D. Linde, and A. A. Starobinsky, *Phys. Rev. Lett.* **73**, 3195 (1994), arXiv:hep-th/9405187.
- [6] Y. Shtanov, J. H. Traschen, and R. H. Brandenberger, *Phys. Rev. D* **51**, 5438 (1995), arXiv:hep-ph/9407247.
- [7] B. A. Bassett, S. Tsujikawa, and D. Wands, *Rev. Mod. Phys.* **78**, 537 (2006), arXiv:astro-ph/0507632.
- [8] A. V. Frolov, *Class. Quant. Grav.* **27**, 124006 (2010), arXiv:1004.3559 [gr-qc].
- [9] R. Allahverdi, R. Brandenberger, F.-Y. Cyr-Racine, and A. Mazumdar, *Ann. Rev. Nucl. Part. Sci.* **60**, 27 (2010), arXiv:1001.2600 [hep-th].
- [10] M. A. Amin, M. P. Hertzberg, D. I. Kaiser, and J. Karouby, *Int. J. Mod. Phys. D* **24**, 1530003 (2014), arXiv:1410.3808 [hep-ph].
- [11] K. D. Lozanov, (2019), arXiv:1907.04402 [astro-ph.CO].
- [12] R. Allahverdi *et al.*, *Open J. Astrophys.* **4**, astro.2006.16182 (2021), arXiv:2006.16182 [astro-ph.CO].
- [13] A. Berera, *Phys. Rev. Lett.* **75**, 3218 (1995), arXiv:astro-ph/9509049.
- [14] M. Bastero-Gil, A. Berera, R. O. Ramos, and J. G. Rosa, *Physical Review Letters* **117**, 151301 (2016).
- [15] V. Kamali, M. Motaharfard, and R. O. Ramos, *Universe* **9**, 124 (2023), arXiv:2302.02827 [hep-ph].
- [16] P. Collaboration, Y. Akrami, F. Arroja, M. Ashdown, J. Aumont, C. Baccigalupi, M. Ballardini, A. Banday, R. Barreiro, N. Bartolo, *et al.*, (2020).
- [17] N. Aghanim *et al.* (Planck), *Astron. Astrophys.* **641**, A6 (2020), arXiv:1807.06209 [astro-ph.CO].
- [18] N. Aghanim *et al.* (Planck), *Astron. Astrophys.* **641**, A5 (2020), arXiv:1907.12875 [astro-ph.CO].
- [19] M. Motaharfard, V. Kamali, and R. O. Ramos, *Phys. Rev. D* **99**, 063513 (2019), arXiv:1810.02816 [astro-ph.CO].
- [20] V. Kamali, *Phys. Rev. D* **100**, 043520 (2019), arXiv:1901.01897 [gr-qc].
- [21] K. V. Berghaus, P. W. Graham, and D. E. Kaplan, *JCAP* **03**, 034 (2020), arXiv:1910.07525 [hep-ph].
- [22] L. Visinelli, *JCAP* **07**, 054 (2016), arXiv:1605.06449 [astro-ph.CO].
- [23] M. Benetti and R. O. Ramos, *Phys. Rev. D* **95**, 023517 (2017), arXiv:1610.08758 [astro-ph.CO].
- [24] N. Videla and G. Panotopoulos, *Phys. Rev. D* **97**, 123503 (2018), arXiv:1710.05046 [gr-qc].
- [25] M. Bastero-Gil, S. Bhattacharya, K. Dutta, and M. R. Gangopadhyay, *JCAP* **02**, 054 (2018), arXiv:1710.10008 [astro-ph.CO].
- [26] R. Arya, A. Dasgupta, G. Goswami, J. Prasad, and R. Rangarajan, *JCAP* **02**, 043 (2018), arXiv:1710.11109 [astro-ph.CO].
- [27] C. Gomes, O. Bertolami, and J. G. Rosa, *Phys. Rev. D* **97**, 104061 (2018), arXiv:1803.08084 [hep-th].
- [28] M. Bastero-Gil, A. Berera, R. Hern3ndez-Jim3nez, and J. a. G. Rosa, *Phys. Rev. D* **98**, 083502 (2018), arXiv:1805.07186 [astro-ph.CO].
- [29] S. Das, *Phys. Rev. D* **99**, 063514 (2019), arXiv:1810.05038 [hep-th].
- [30] M. Bastero-Gil, A. Berera, and J. R. Calder3n, *JCAP* **07**, 019 (2019), arXiv:1904.04086 [astro-ph.CO].
- [31] G. Montefalcone, V. Aragam, L. Visinelli, and K. Freese, *Phys. Rev. D* **107**, 063543 (2023), arXiv:2209.14908 [gr-qc].
- [32] G. Montefalcone, V. Aragam, L. Visinelli, and K. Freese, *JCAP* **03**, 002 (2023), arXiv:2212.04482 [gr-qc].
- [33] S. Das and R. O. Ramos, *Universe* **9**, 76 (2023), arXiv:2212.13914 [astro-ph.CO].
- [34] A. Mukuno and J. Soda, *Phys. Rev. D* **109**, 123504 (2024), arXiv:2402.08849 [hep-th].
- [35] U. Kumar and S. Das, *JCAP* **10**, 058 (2024), arXiv:2407.06032 [astro-ph.CO].
- [36] W. DeRocco, P. W. Graham, and S. Kalia, *JCAP* **11**, 011 (2021), arXiv:2107.07517 [hep-ph].
- [37] M. Laine and S. Proccacci, *JCAP* **06**, 031 (2021), arXiv:2102.09913 [hep-ph].
- [38] K. V. Berghaus, M. Drewes, and S. Zell, (2025), arXiv:2503.18829 [hep-ph].
- [39] R. O. Ramos and G. S. Rodrigues, (2025), arXiv:2504.20943 [hep-ph].
- [40] E. Broadberry, A. Hook, and S. Mondal, (2025), arXiv:2505.07943 [hep-ph].
- [41] S. Bhattacharya, M. Fasiello, A. Papageorgiou, and E. Dimastrogiovanni, (2025), arXiv:2506.11853 [astro-ph.CO].
- [42] R. Z. Ferreira and A. Notari, *JCAP* **09**, 007 (2017), arXiv:1706.00373 [astro-ph.CO].
- [43] L. Visinelli, *JCAP* **09**, 013 (2011), arXiv:1107.3523 [astro-ph.CO].
- [44] ().
- [45] ().

- [46] H. Mishra, S. Mohanty, and A. Nautiyal, *Phys. Lett. B* **710**, 245 (2012), arXiv:1106.3039 [hep-ph].
- [47] V. Kamali and R. O. Ramos, *JCAP* **01**, 048 (2025), arXiv:2410.22624 [hep-ph].
- [48] R. Z. Ferreira and A. Notari, *Phys. Rev. D* **97**, 063528 (2018), arXiv:1711.07483 [astro-ph.CO].
- [49] S. Hassan, G. R. Kane, J. March-Russell, and G. Obied, *JHEP* **03**, 022 (2025), arXiv:2410.19906 [hep-ph].
- [50] T. Fujita, K. Mukaida, and T. Tsuji, (2025), arXiv:2503.01228 [hep-ph].
- [51] M. Bellac, *Thermal Field Theory, Cambridge Monographs on Mathematical Physics*, (Cambridge University Press, 2011).
- [52] L. D. McLerran, E. Mottola, and M. E. Shaposhnikov, *Phys. Rev. D* **43**, 2027 (1991).
- [53] S. Y. Khlebnikov, *Phys. Rev. D* **46**, R3223 (1992).
- [54] M. M. Anber and L. Sorbo, *Phys. Rev. D* **81**, 043534 (2010), arXiv:0908.4089 [hep-th].
- [55] N. Barnaby, R. Namba, and M. Peloso, *JCAP* **04**, 009 (2011), arXiv:1102.4333 [astro-ph.CO].
- [56] N. Barnaby and M. Peloso, *Phys. Rev. Lett.* **106**, 181301 (2011), arXiv:1011.1500 [hep-ph].
- [57] J. L. Cook and L. Sorbo, *Phys. Rev. D* **85**, 023534 (2012), [Erratum: *Phys. Rev. D* **86**, 069901 (2012)], arXiv:1109.0022 [astro-ph.CO].
- [58] O. Özsoy, K. Sinha, and S. Watson, *Phys. Rev. D* **91**, 103509 (2015), arXiv:1410.0016 [hep-th].
- [59] S.-L. Cheng, W. Lee, and K.-W. Ng, *Phys. Rev. D* **93**, 063510 (2016), arXiv:1508.00251 [astro-ph.CO].
- [60] M. Peloso, L. Sorbo, and C. Unal, *JCAP* **09**, 001 (2016), arXiv:1606.00459 [astro-ph.CO].
- [61] E. V. Gorbar, K. Schmitz, O. O. Sobol, and S. I. Vilchinskii, *Phys. Rev. D* **104**, 123504 (2021), arXiv:2109.01651 [hep-ph].
- [62] R. Durrer, R. von Eckardstein, D. Garg, K. Schmitz, O. Sobol, and S. Vilchinskii, *Phys. Rev. D* **110**, 043533 (2024), arXiv:2404.19694 [astro-ph.CO].
- [63] S. P. Corbà and L. Sorbo, *JCAP* **10**, 024 (2024), arXiv:2403.03338 [astro-ph.CO].
- [64] D. Jiménez, K. Kamada, K. Schmitz, and X.-J. Xu, *JCAP* **12**, 011 (2017), arXiv:1707.07943 [hep-ph].
- [65] V. Domcke, V. Guidetti, Y. Welling, and A. Westphal, *JCAP* **09**, 009 (2020), arXiv:2002.02952 [astro-ph.CO].
- [66] M. Peloso and L. Sorbo, *JCAP* **01**, 038 (2023), arXiv:2209.08131 [astro-ph.CO].
- [67] J. Garcia-Bellido, A. Papageorgiou, M. Peloso, and L. Sorbo, *JCAP* **01**, 034 (2024), arXiv:2303.13425 [astro-ph.CO].
- [68] R. von Eckardstein, M. Peloso, K. Schmitz, O. Sobol, and L. Sorbo, *JHEP* **11**, 183 (2023), arXiv:2309.04254 [hep-ph].
- [69] K. Alam, K. Dutta, and N. Jaman, *JCAP* **12**, 015 (2024), arXiv:2405.10155 [astro-ph.CO].
- [70] J.-F. He, K.-G. Zhang, C. Fu, and Z.-K. Guo, (2025), arXiv:2502.13158 [hep-ph].
- [71] D. G. Figueroa, J. Lizarraga, A. Urío, and J. Urrestilla, *Phys. Rev. Lett.* **131**, 151003 (2023), arXiv:2303.17436 [astro-ph.CO].
- [72] R. Sharma, A. Brandenburg, K. Subramanian, and A. Vikman, *JCAP* **05**, 079 (2025), arXiv:2411.04854 [astro-ph.CO].
- [73] A. Caravano, E. Komatsu, K. D. Lozanov, and J. Weller, *Phys. Rev. D* **105**, 123530 (2022), arXiv:2110.10695 [astro-ph.CO].
- [74] Y.-L. Wu, L.-S. Liu, L.-H. Sui, Y.-F. Wang, X.-B. Li, and N. Bai, *Phys. Rev. D* **108**, 123502 (2023).
- [75] M. Bastero-Gil, A. Berera, and R. O. Ramos, *JCAP* **09**, 033 (2011), arXiv:1008.1929 [hep-ph].
- [76] Y. Akrami *et al.* (Planck), *Astron. Astrophys.* **641**, A10 (2020), arXiv:1807.06211 [astro-ph.CO].
- [77] T. Louis *et al.* (ACT), (2025), arXiv:2503.14452 [astro-ph.CO].
- [78] A. Lewis, A. Challinor, and A. Lasenby, *Astrophys. J.* **538**, 473 (2000), arXiv:astro-ph/9911177.
- [79] C. Howlett, A. Lewis, A. Hall, and A. Challinor, *JCAP* **04**, 027 (2012), arXiv:1201.3654 [astro-ph.CO].
- [80] N. Aghanim *et al.* (Planck), *Astron. Astrophys.* **641**, A8 (2020), arXiv:1807.06210 [astro-ph.CO].
- [81] S. Alam *et al.* (BOSS), *Mon. Not. Roy. Astron. Soc.* **470**, 2617 (2017), arXiv:1607.03155 [astro-ph.CO].
- [82] A. Lewis and S. Bridle, *Phys. Rev. D* **66**, 103511 (2002), arXiv:astro-ph/0205436.
- [83] A. Lewis, *Phys. Rev. D* **87**, 103529 (2013), arXiv:1304.4473 [astro-ph.CO].
- [84] A. Lewis, (2019), arXiv:1910.13970 [astro-ph.IM].
- [85] E. Dimastrogiovanni, M. Fasiello, J. M. Leedom, M. Putti, and A. Westphal, *JHEP* **08**, 072 (2024), arXiv:2312.13431 [hep-th].
- [86] A. Papageorgiou, P. Quílez, and K. Schmitz, *JHEP* **01**, 169 (2023), arXiv:2206.01129 [hep-ph].

Appendix A: Estimatio of the dissipation coefficient

The dissipation coefficient Υ plays a critical role in understanding the dynamics of a scalar field ϕ interacting with other fields X . If the potential is given as:

$$V(\phi, X) = V(\phi) + V_{\text{int}}(\phi, X),$$

where the interaction term is:

$$V_{\text{int}}(\phi, X) = f(\phi)g(X).$$

then the effective equation of motion for ϕ becomes:

$$\frac{\partial}{\partial \mu} \frac{\partial \mathcal{L}_{\text{eff}}}{\partial (\partial_\mu \phi)} - \frac{\partial \mathcal{L}_{\text{eff}}}{\partial \phi} - i \frac{\partial f(\phi)}{\partial \phi} \int d^4 x' \theta(t-t') \times [f(\phi(x')) - f(\phi(x))] \langle [g(X(x)), g(X(x'))] \rangle = 0.$$

With the adiabatic approximation $\frac{\dot{\phi}}{\phi} \ll \tau^{-1}$, the field's evolution is slow compared to the system's response timescale τ [75].

Expanding $f(\phi)$ to estimate the causal effect at a time t' around time t using a Taylor series

$$f(\phi(t')) - f(\phi(t)) \approx (t' - t) \dot{\phi}(t) \frac{\partial f(\phi)}{\partial \phi},$$

and incorporating dissipative terms, leads to the effective equation of motion Eq. (9). The dissipation coefficient Υ is defined as:

$$\Upsilon = \int d^4 x' \Sigma_R(x, x')(t' - t).$$

The retarded correlation function $\Sigma_R(x, x')$ is given by:

$$\Sigma_R(x, x') = -i \left[\frac{\partial f(\phi)}{\partial \phi} \right]^2 \theta(t - t') \langle [g(X(x)), g(X(x'))] \rangle.$$

These equations describe how energy dissipates from the scalar field ϕ into coupled fields X , significantly influencing the field's return to equilibrium.

The retarded Green's function for an operator $O(t, \mathbf{x})$ is defined as:

$$\Sigma_R(t - t', \mathbf{x} - \mathbf{x}') = i \Theta(t - t') \langle [O(t, \mathbf{x}), O(t', \mathbf{x}')] \rangle,$$

where $\Theta(t - t')$ is the Heaviside step function, ensuring causality. This definition captures the causal response of the system to a perturbation at t' .

To study the Green's function in momentum space, we take the Fourier transform:

$$\Sigma_R(t - t', \mathbf{x} - \mathbf{x}') = \int \frac{d\omega}{2\pi} e^{-i\omega(t-t')} \int \frac{d^3 k}{(2\pi)^3} e^{i\mathbf{k} \cdot (\mathbf{x} - \mathbf{x}')} \tilde{G}^R(\omega, \mathbf{k}).$$

The thermal average of $O(t, \mathbf{x})O(t', \mathbf{x}')$ can be expanded using the eigenstates $|n\rangle$ and $|m\rangle$ of the unperturbed Hamiltonian:

$$\langle O(t, \mathbf{x})O(t', \mathbf{x}') \rangle = \sum_{n,m} \langle n | O(t, \mathbf{x}) | m \rangle \langle m | O(t', \mathbf{x}') | n \rangle e^{-\beta E_n}.$$

Substituting $O(t, \mathbf{x}) = e^{iHt - i\mathbf{P} \cdot \mathbf{x}} O(0, 0) e^{-iHt + i\mathbf{P} \cdot \mathbf{x}}$, we can write:

$$\langle O(t, \mathbf{x})O(t', \mathbf{x}') \rangle = \sum_{n,m} e^{-i(E_m - E_n)(t-t') + i(\mathbf{p}_m - \mathbf{p}_n) \cdot (\mathbf{x} - \mathbf{x}')} \times e^{-\beta E_n} |\langle n | O(0, 0) | m \rangle|^2.$$

The commutator $\langle [O(t, \mathbf{x}), O(t', \mathbf{x}')] \rangle$ therefore becomes:

$$\langle [O(t, \mathbf{x}), O(t', \mathbf{x}')] \rangle = \sum_{n,m} e^{-i(E_m - E_n)(t-t') + i(\mathbf{p}_m - \mathbf{p}_n) \cdot (\mathbf{x} - \mathbf{x}')} \times e^{-\beta E_n} (1 - e^{-\beta \omega}) |\langle n | O(0, 0) | m \rangle|^2,$$

where $\omega = E_m - E_n$.

Taking the Fourier transform of the commutator gives:

$$\begin{aligned} \rho_0(\omega, \mathbf{k}) &\equiv \text{FT}(\langle [O(t, \mathbf{x}), O(t', \mathbf{x}')] \rangle) \\ &= (1 - e^{-\beta \omega}) \text{FT}(\langle O(t, \mathbf{x})O(t', \mathbf{x}') \rangle), \end{aligned}$$

where the Bose-Einstein distribution $n_B(\omega) = 1/(e^{\beta \omega} - 1)$ relates the occupation of states to temperature.

$\rho_0(\omega, \mathbf{k})$ is the spectral density function for the operator O . This function encapsulates the thermal behavior of the system and is essential for determining the plasma's retarded Green's function. The spectral density function for our case is then evaluated with the prescription of [49], leading to the expression in Eq. (12).

Appendix B: Detailed results for posterior distributions and additional plots

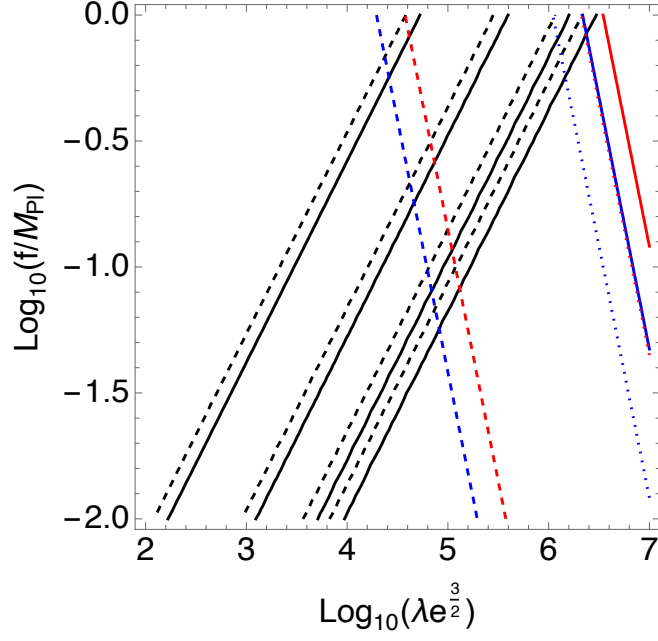


FIG. 6: Contour plot for Q for $Q = 1, 10, 50, 100$ are shown with $\lambda e^{3/2}$ and f for $N_{\text{inf}} = 50$ (dashed black lines) and $N_{\text{inf}} = 60$ (solid black lines). Red and blue lines are the same *constraint contours* as in Fig. 4.

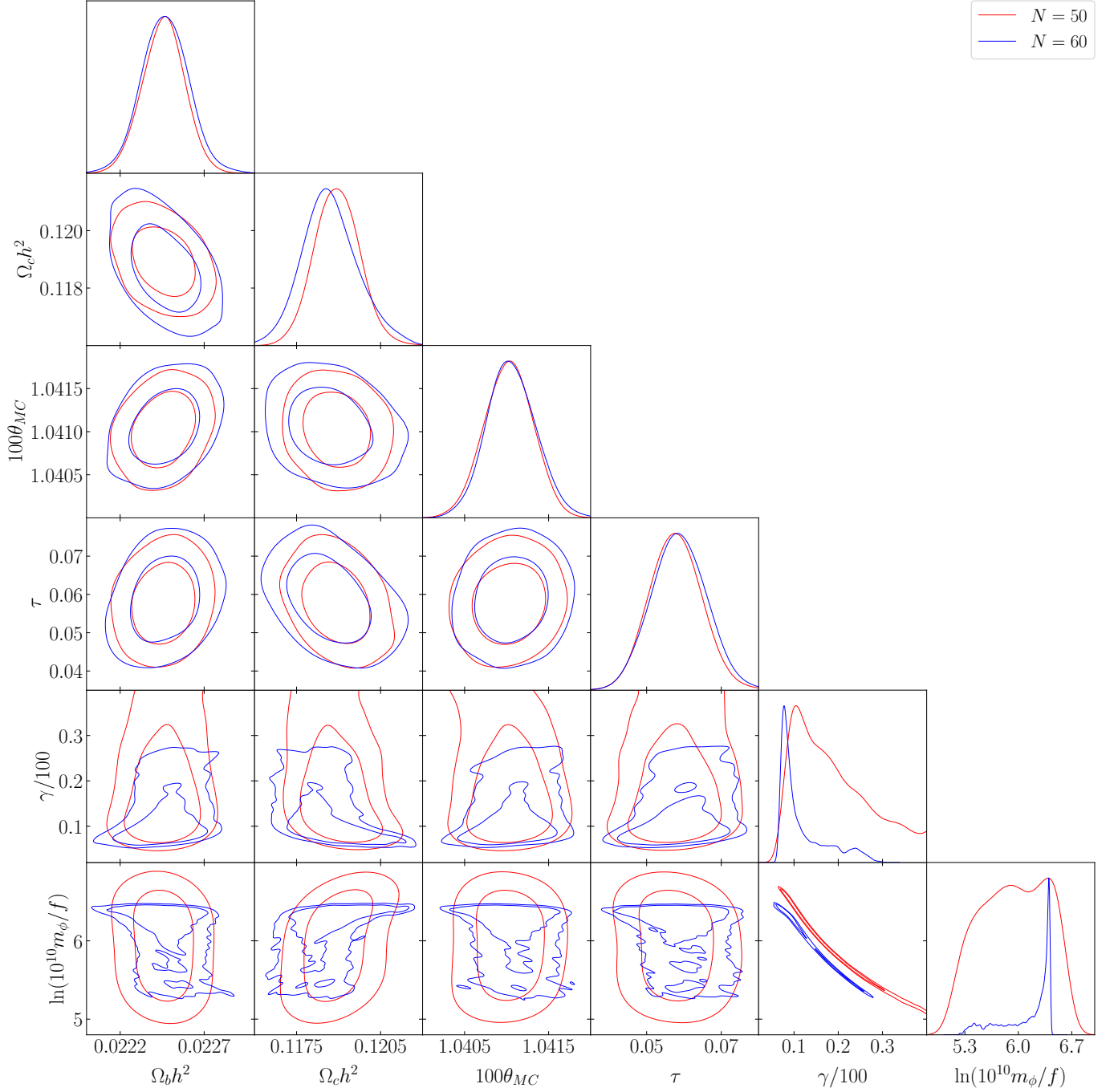


FIG. 7: Posterior distributions for all parameters.

Parameter	$N_{\text{inf}} = 50$	$N_{\text{inf}} = 60$
$\Omega_b h^2$	0.02245 ± 0.00012 (0.02246)	0.02247 ± 0.00014 (0.02247)
$\Omega_c h^2$	0.11895 ± 0.00081 (0.11913)	0.11870 ± 0.00101 (0.11904)
$100\theta_{MC}$	1.04102 ± 0.00028 (1.04089)	1.04106 ± 0.00029 (1.04113)
τ	0.05779 ± 0.00700 (0.05789)	0.05866 ± 0.00752 (0.05555)
$\ln(10^{10} m_\phi / f)$	5.94695 ± 0.44071 (6.12459)	6.12390 ± 0.33225 (6.37145)
$\gamma/100$	0.18592 ± 0.08613 (0.14199)	0.11872 ± 0.05517 (0.08042)

TABLE II: Mean values with 68% limits of all the parameters. The corresponding best-fit values are given in brackets.